Characterization of nighttime formation of particulate organic nitrates based on high-resolution aerosol mass spectrometry in an urban atmosphere in China

Kuangyou Yu[1,2,*], Qiao Zhu[1,*], Ke Du[2], Xiao-Feng Huang[1]

[1]Key Laboratory for Urban Habitat Environmental Science and Technology, School of Environment and Energy, Peking University Shenzhen Graduate School, Shenzhen, 518055, China.

[2]Department of Mechanical and Manufacturing Engineering, University of Calgary, Calgary, Canada.

* Authors have equal contribution.

Abstract. Organic nitrates are important atmospheric species that significantly affect the cycling of NOx and ozone production. However, characterization of particulate organic nitrates and their sources in polluted atmosphere is a big challenge and has not been comprehensively studied in Asia. In this study, an Aerodyne high-resolution time-of-flight aerosol mass spectrometer (HR-ToF-AMS) was deployed at an urban site in China from 2015 to 2016 to characterize particulate organic nitrates in total nitrates with high time resolution. Based on the cross validation of two different data processing methods, organic nitrates were effectively quantified to contribute a notable fraction of organic aerosol (OA): 9-21% in spring, 11-25% in summer, 9-20% in autumn, while very small fraction in winter. The good correlation between organic nitrates and fresh secondary organic aerosol (SOA) at night, as well as the diurnal trend of size distribution of organic nitrates, indicated a key role of nighttime local secondary formation of organic nitrates in Shenzhen. Furthermore, theoretical calculations of nighttime SOA production of NO_3 reactions with volatile organic compounds (VOCs) measured during the spring campaign were performed, resulting in three biogenic VOCs (α-pinene, limonene, and camphene) and one anthropogenic VOC (styrene) identified as the possible key VOC precursors for particulate organic nitrates. The comparison with similar studies in the literature implied that nighttime particulate organic nitrates formation is highly relevant with NOx levels. This study proposes that unlike the documented cases in the United States and Europe, modeling nighttime particulate organic nitrate formation in China should incorporate not only biogenic VOCs but also anthropogenic VOCs for urban air pollution, which needs the support of relevant smog chamber studies in the future.

Correspondence to: X.-F. Huang (huangxf@pku.edu.cn)

1. Introduction

Organic nitrates (ON) in aerosols have an important impact on the fate of NO_X and ozone production (Lelieveld et al., 2016), which can be formed in a minor channel of the reaction between peroxy radicals and NO (R1 and R2) (usually, an increased fraction of this reaction leads to the formation of alkoxy radicals and NO_2 (R3)) or via the NO_3-induced oxidation of unsaturated hydrocarbons (R4). Even though some recent studies have suggested that the formation of organic nitrates from peroxy radicals and NO may play a larger role than previously recognized (Teng et al., 2015, 2017), yields of organic nitrates via NO_3 reacting with alkenes are generally much higher (Fry et al., 2009; Ayres et al., 2015; Boyd et al.,2015,2017).

$$RH + OH + O_2 \rightarrow RO_2 + H_2O \quad (R1)$$
$$RO_2 + NO \rightarrow RONO_2 \quad (R2)$$
$$RO_2 + NO \rightarrow RO + NO_2 \quad (R3)$$
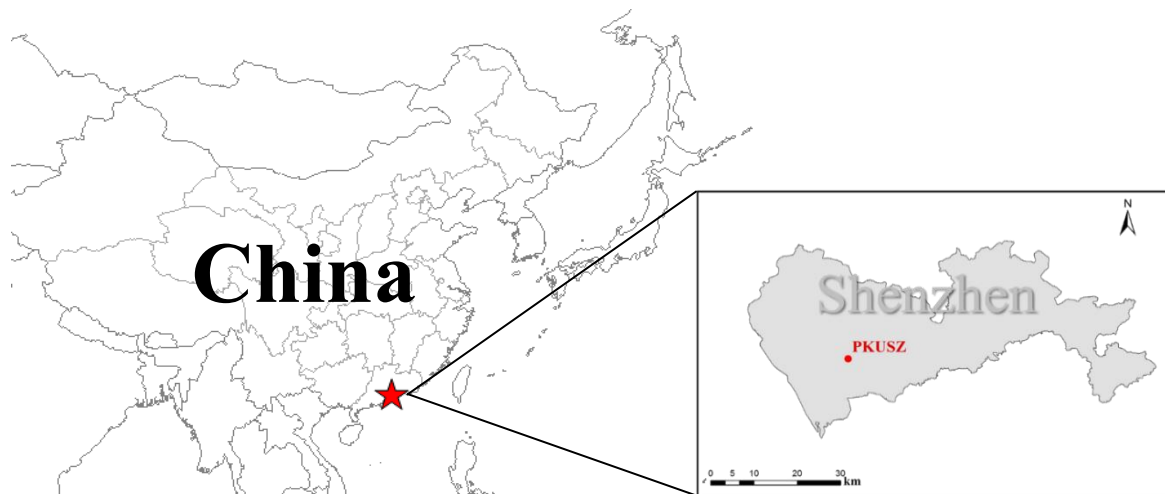$$R = R' + NO_3 \rightarrow R(ONO_2)\ R' \quad (R4)$$

Several methods have been developed to directly measure total organic nitrates (gas + particle) in the real atmosphere. For example, Rollins et al.(2012) used a thermal-dissociation laser-induced fluorescence technique (TD-LIF) to observe organic nitrates in the United States; Sobanski et al. (2017) measured organic nitrates in Germany using the thermal dissociation cavity ring-down spectroscopy (TD-CRDS). Field and laboratory studies around the world indicated that particulate organic nitrates could contribute a large portion of secondary organic aerosol (SOA) (Rollins et al., 2012; Xu et al., 2015a; Fry et al., 2013; Ayres et al., 2015; Boyd et al., 2015; Lee et al., 2016). Recently, researchers have proposed some estimation methods for particle-phase organic nitrates based on aerosol mass spectrometry (AMS) with high time resolution (Farmer et al., 2010; Hao et al., 2014; Xu et al., 2015a, 2015b). Ng et al. (2017) reviewed the nitrate radical chemistry and the abundance of particulate organic nitrates in the United States and Europe, and further concluded that particulate organic nitrates are formed substantially via NO_3+BVOC chemistry, which plays an important role in SOA formation. Unfortunately, relevant Chinese datasets are scarce yet and not included in this review. This was because (1) the contributions of organic nitrates in SOA and total nitrates in Chinese atmosphere remain poorly understood; (2) the anthropogenic and biogenic precursor emissions in China are significantly different from those in the United States and Europe, and thus cannot be easily estimated. To our best knowledge, few studies have investigated the concentrations and formation pathways of particulate organic nitrates in China. Xu et al. (2017) estimated the mass concentration of organic nitrogen in Beijing using AMS, but in this study they ignored the contribution of NO_X^+ family, which are the major fragments of organic nitrates.

Shenzhen is a megacity of China in a subtropical region, where NOx involved photochemical reactions are very active, given considerable biogenic and anthropogenic VOC emissions (Zhang et al., 2008). To assess the evolution of particulate organic nitrates in a polluted urban atmosphere, we deployed an Aerodyne high-resolution time-of-flight aerosol mass spectrometer (HR-ToF-AMS) and other instruments in Shenzhen from 2015 to 2016 in this study. Organic nitrates and their contributions to OA in different seasons were estimated by different methods using the HR-ToF-AMS datasets, based on which, the secondary formation pathway of particulate organic nitrates in Shenzhen was further explored.

2. Experiment methods

2.1 Sampling site and period

The sampling site (22.6°N, 113.9°E) was on the roof (20 m above ground) of an academic building on the campus of Peking University Shenzhen Graduate School (PKUSZ), which is located in the western urban area in Shenzhen (Figure 1). This site is mostly surrounded by subtropical plants without significant anthropogenic emission sources nearby, except a local road that is ~100 m from the site. In this study, we used the statistical data from the Meteorological Bureau of Shenzhen Municipality (http://www.szmb.gov.cn/site/szmb/Esztq/index.html) as the reference data to determine the sampling periods for four different seasons during 2015-2016, as shown in Table 1.

Figure 1. The location of the sampling site.

Table 1. Meteorological conditions, PM_1 species concentrations and relevant parameters for different sampling periods in Shenzhen.

| | Sampling period | 4.1-4.30, 2016 | 8.1-8.31, 2015 | 11.4-11.30, 2015 | 1.21-2.3, 2016 |
		Spring	Summer	Autumn	Winter
Meteorology	T (°C)	24.5±2.5	29.0±3.0	23.6±3.7	10.7±4.7
	RH (%)	78.0±12.7	71.2±17.5	68.2±15.8	75.4±18.7
	WS (m s^{-1})	1.4±0.8	1.0±0.7	1.2±0.7	1.5±0.8
Species	Org	4.3±3.2	10.0±6.9	7.8±5.9	5.1±3.5
	SO_4^{2-}	3.2±1.8	5.8±3.3	2.3±1.5	1.9±1.2
	Total NO_3^-	0.96±1.4	0.91±0.90	1.3±1.4	1.6±1.0

(µg m^{-3})	NH_4^+	1.4±0.8	2.0±1.1	1.1±0.8	1.2±0.6
	Cl^-	0.14±0.19	0.03±0.05	0.22±0.36	0.64±0.85
	BC	1.9±2.1	2.4±1.6	3.5±2.6	2.4±1.5
	Total	12.0±8.9	15.1±13.8	11.8±9.5	12.2±7.2
ON relevant parameters	R_{NH4NO3}	2.80	3.20	3.32	3.48
	R_{obs}	3.74	6.14	4.30	3.55
	Fraction of positive numbers of R_{obs}- R_{NH4NO3}	99%	99%	84%	47%

2.2 Instrumentation

2.2.1 High Resolution Time-of-Flight Aerosol Mass Spectrometer

During the sampling periods, chemical composition of non-refractory PM$_1$ was measured by an Aerodyne HR-ToF-AMS, and detailed descriptions of this instrument are given in the literature (DeCarlo et al., 2006; Canagaratna et al., 2007). The setup and operation of the HR-ToF-AMS can be found in our previous publications (Huang et al., 2010, 2012; Zhu et al.,2016). To remove coarse particles, a PM$_{2.5}$ cyclone inlet was installed before the sampling copper tube with a flow rate of 10 l min^{-1}. Before entering the AMS, the sampled air was dried by a nafion dryer (MD-070-12S-4, Perma Pure Inc.) to eliminate the potential influence of relative humidity on particle collection (Matthew et al., 2008). The ionization efficiency (IE) calibrations were performed using pure ammonium nitrate every two weeks. The relative ionization efficiencies (RIEs) used in this study were 1.2 for sulfate, 1.1 for nitrate, 1.3 for chloride, 1.4 for organics and 4.0 for ammonium, respectively (Jimenez et al., 2003). Composition-dependent collection efficiencies (CEs) were applied to the data according to the method in Middlebrook et al. (2012). The instrument was operated at two ion optical modes with a cycle of 4 min, including 2 min for the mass-sensitive V-mode and 2 min for the high mass resolution W-mode. The HR-ToF-AMS data analysis was performed using the software SQUIRREL (version 1.57) and PIKA (version 1.16) written in Igor Pro 6.37 (Wave Metrics Inc.) (http://cires1.colorado.edu/jimenezgroup/ToFAMSResources/ToFSoftware / index.html).

2.2.2 Other co-located instruments

In addition to the HR-ToF-AMS, other relevant instruments were deployed at the same sampling site. An aethalometer (AE-31, Magee) was used for measurement of refractory black carbon (BC) with a resolution of 5 min. An SMPS system (3775 CPC and 3080 DMA, TSI Inc.) was used to obtain the particle number size distribution in 15–615 nm (mobility diameter) with a time resolution of 5 min. Ozone and NO$_X$ were measured by a 49i ozone analyzer and a 42i nitrogen oxide analyzer (Thermo Scientific), respectively. In the spring campaign, ambient VOC concentrations were also measured using an on-line VOC monitoring system (TH-300B, Tianhong Corp.), including an ultralow-temperature preconcentration cold trap and an

automated in-situ gas chromatograph (Agilent 7820A) equipped with a mass spectrometer (Agilent 5977E). The system had both a flame ionization detector (FID) gas channel for C2–C5 hydrocarbons and a mass spectrometer (MS) gas channel for C5–C12 hydrocarbons, halohydrocarbons and oxygenated VOCs. A complete working cycle of the system was one hour and included six steps: sample collection, freeze-trapping, thermal desorption, GC-FID/MS analysis, heating and anti-blowing purification. The sample collection time was 5 min. The sampling flow speed was 60 ml min^{-1}. The anti-blowing flow speed was 200 ml min^{-1}. The calibration of over 100 VOCs was performed using mixed standard gas before and after the campaign. Detection limits for most compounds were near 5 pptv. More description of this instrument can be found in Wang et al. (2014).

2.3 Organic nitrates estimation methods

In this study, we used two independent methods to estimate particulate organic nitrates based on the AMS data, following the approaches in Xu et al. (2015b). The first method is based on the NO^+/NO_2^+ ratio (NO_X^+ ratio) in the HR-AMS spectrum. Due to the very different NO_X^+ ratios of organic nitrates and inorganic nitrate (i.e., R_{ON} and R_{NH4NO3}, respectively) (Farmer et al., 2010; Boyd et al., 2015; Fry et al., 2008; Bruns et al., 2010), the NO_2^+ and NO^+ concentrations of organic nitrates ($NO_{2,ON}$ and NO_{ON}) can be quantified with the HR-AMS data via Eqs. (1) and (2), respectively (Farmer et al., 2010):

$$NO_2^+{}_{,ON} = \frac{NO_2^+{}_{,obs} \times (R_{obs} - R_{NH4NO3})}{R_{ON} - R_{NH4NO3}} \quad (1)$$

$$NO^+{}_{ON} = R_{ON} \times NO_{2,ON} \quad (2)$$

where R_{obs} is the NO_X^+ ratio from the observation. The value of R_{ON} is difficult to determine because it varies between instruments and precursor VOCs. However, R_{NH4NO3} was determined by IE calibration using pure NH_4NO_3 every two weeks for each campaign and the results showed stable values: In spring, the average R_{NH4NO3} was 2.66 for the first IE calibration and 2.94 for the second one; in summer, the average R_{NH4NO} was 3.05 and 3.34 for the first and second IE calibrations, respectively; in autumn, the average R_{NH4NO3} was 3.33 and 3.31 for the first and second IE calibrations, respectively; in winter, the average R_{NH4NO3} was 3.45 and 3.51 for the first and second IE calibrations, respectively. We adopted the R_{ON}/R_{NH4NO3} estimation range (from 2.08 to 3.99) for variation of precursor VOCs in the literature to determine R_{ON} (Farmer et al., 2010; Boyd et al., 2015; Bruns et al., 2010; Sato et al., 2010; Xu et al., 2015b), and thus two R_{ON} values were calculated for each season to provide the upper bound ($NO_{3\_org\_ratio\_1}$) and lower bound ($NO_{3\_org\_ratio\_2}$) of $NO_{3,org}$ mass concentration.

The second method is based on the traditional positive matrix factorization (PMF) analysis of HR organic mass spectra, which resolves different organic factors (Zhang et al., 2011; Ng et al., 2010; Huang et al., 2013). Combined with NO^+ and NO_2^+ ions, the same analysis of HR organic mass spectra was performed to separate NO^+ and NO_2^+ ions into different organic factors and an inorganic nitrate factor (Hao et al., 2014; Xu et al., 2015b). The PMF analysis procedures in this study can be found in our previous publications (Huang et al., 2010; Zhu et al., 2016; He et al., 2011), resulting in three organic factors and one inorganic factor in spring, summer and autumn: a hydrocarbon-like OA (HOA) characterized by $C_nH_{2n+1}^+$ and $C_nH_{2n-1}^+$ and O/C of 0.11 to 0.18, a less-oxidized oxygenated OA (LO-OOA) characterized by $C_xH_yO_z^+$ especially $C_2H_3O^+$ and O/C of 0.28 to 0.70, a more-oxidized oxygenated OA (MO-OOA) also characterized by $C_xH_yO_z^+$ especially CO_2^+ and O/C of 0.78 to 1.24, and a

128   nitrate inorganic aerosol (NIA) characterized by overwhelming NO^+ and NO_2^+, as indicated in Fig S6. According to the

129   diagnostic plots of the PMF analysis shown in Figure S2 to S4, the same organic factors as those in the traditional PMF analysis

130   of only organic mass spectra were obtained. The NO^+ and NO_2^+ ions were distributed among different OA factors and the NIA

131   factor; thus the concentrations of nitrate functionality (NO_{org}^+ and $NO_{2,org}^+$) in organic nitrates ($NO_{3, org}$) are equal to the sum of

132   NO_2^+ and NO^+ via Eqs. (3) and (4), respectively (Xu et al., 2015b):

$$NO_{2,org}^+ = \sum([OA\ factor]_i \times f_{NO2,i}) \quad (3)$$

$$NO_{org}^+ = \sum([OA\ factor]_i \times f_{NO,i}) \quad (4)$$

135   where [*OA factor*]$_i$ represents the mass concentration of OA factor i, and $f_{NO2,i}$ and $f_{NO,i}$ represent the mass fractions of NO_2^+

136   and NO^+, respectively.

137   It should be noted that the 4-factor solution seemed to have a "mixed factor" problem to some extent (Zhu et al., 2018). For

138   example, HOA mixed with COA (clear $C_3H_3O^+$ in m/z 55 for spring, summer and autumn) (Mohr et al., 2012), and BBOA

139   mixed with LO-OOA (clear m/z 60 and 73 signals in LO-OOA in autumn) (Cubison et al., 2011). However, running PMF with

140   more factors would produce unexplained factors but less influence on the apportionment of NO^+ and NO_2^+ ions between

141   organic nitrates and inorganic nitrate (Table S1). In addition, the standard deviations of NO^+ and NO_2^+ ions in the OA factors

142   across different FPEAK values (from −1.0 to 1.0) were very small (Table S2). Therefore, the 4-factor solution was used for

143   quantifying organic nitrates in spring, summer and autumn.

3. Results and discussion

3.1 Organic nitrates estimation

146   Table 2 shows the concentrations of nitrate functionality in organic nitrates (i.e., $NO_{3, org}$), estimated by both the NO^+/NO_2^+

147   ratio method and PMF method, as well as their contributions to the total measured nitrate. It should be noted that the small

148   difference between the average R_{obs} and R_{NH4NO3} in winter leads to a large portion of negative data using the NO^+/NO_2^+ ratio

149   method (Table 1). The result from the PMF method shows that the contribution of organic nitrates in total nitrates is only 4.2%

150   in winter (Figure S6), suggesting a negligible contribution of organic nitrates. Thus, we will only discuss organic nitrate

151   estimation results in spring, summer and autumn. The analytical outcomes by the NO^+/NO_2^+ ratio method and by the PMF

152   method consistently suggest that organic nitrates had the highest ambient concentration (0.34-0.53 µg m^{-3}) and proportion in

153   total nitrates (41-64%) in summer among the different seasons. This finding agrees with the finding in (Ng et al., 2017) and it

154   implies a seasonal trend in comparison with that of total nitrates in Table 1. Assuming the average molecular weight of organic

155   nitrates of 200 to 300 g mol^{-1} (Rollins et al., 2012), we found that organic nitrates contributed 9-21% to OA in spring, 11-25%

156   in summer, and 9-20% in autumn.

157   In the PMF method, the mass fractions of organic nitrates in HOA, LO-OOA and MO-OOA were 31%, 49% and 20%,

158   respectively, in spring; 28%, 52% and 20%, respectively, in summer; 30%, 46% and 24%, respectively, in autumn. The major

159 fraction of organic nitrates occurring in LO-OOA for the three seasons implied that organic nitrates were mostly related to
160 fresher secondary OA formation. The NIA factors in all seasons were dominated by but are not limited to NO^+ and NO_2^+.
161 Some organic fragments, such as CO_2^+ and $C_2H_3O^+$, are also part of these factors, which agreed with the findings in the
162 literature (Hao et al., 2014; Xu et al., 2015b; Sun et al., 2012). This indicated the potential interference of organics in the NIA
163 factor. It is also worth to be noted that the NO^+/NO_2^+ ratios in NIA (2.93 for spring, 3.53 for summer and 3.54 for autumn)
164 were higher than that for pure NH_4NO_3 (Table 1), indicating an underestimation of $NO_{3.org}$ concentration by the PMF method.
165 This finding may also explain the reason that the concentration of $NO_{3.org}$ estimated using the PMF method was always close
166 to the lower estimation bound of $NO_{3.org}$ concentration estimated using the NO^+/NO_2^+ ratio method in each season (Table 2).

167 **Table 2.** Summary of organic nitrates estimations using the NO^+/NO_2^+ ratio method and the PMF method

Sampling period	NO^+/NO_2^+ ratio method				PMF method	
	$NO_{3,org}$ (µg m^{-3})[a]		$NO_{3,org}/NO_3$		$NO_{3,org}$ (µg m^{-3})[b]	$NO_{3,org}/NO_3$
	lower	upper	lower	upper		
Spring	0.12	0.19	13%	21%	0.12	12%
Summer	0.34	0.53	41%	64%	0.39	43%
Autumn	0.21	0.33	16%	25%	0.21	16%
Winter	/	/	/	/	0.07	4.2%

168 [a] $NO_{3, org}$ for upper bound is denoted as $NO_{3\_org\_ratio\_1}$, and $NO_{3, org}$ for lower bound is denoted as $NO_{3\_org\_ratio\_2}$.
169 [b] $NO_{3, org}$ estimated using the PMF method is denoted as $NO_{3\_org\_PMF}$.

170 To further verify the reliability of the estimated results of organic nitrates, the $NO_{3, org}$ concentration time series calculated by
171 the two methods in each season are shown in Figure 2a. The computed correlation coefficients (R) are good (0.82 for spring,
172 0.82 for summer and 0.77 for autumn), indicating that similar results were achieved. The inorganic nitrate (NO_{3_inorg*}) obtained
173 by subtracting $NO_{3\_org\_ratio\_1}$ from total measured nitrates also correlated well with the inorganic nitrate estimated using the
174 PMF method (R=0.92 for spring, 0.87 for summer and 0.86 for autumn). While they were distinctive from those of inorganic
175 nitrate (Figure 2b), which indicates that organic nitrates had been well separated from inorganic nitrate in this study, the diurnal
176 trends of organic nitrates obtained by the two methods were similar in each season, with lower concentrations in the daytime
177 and higher concentrations at night.

8
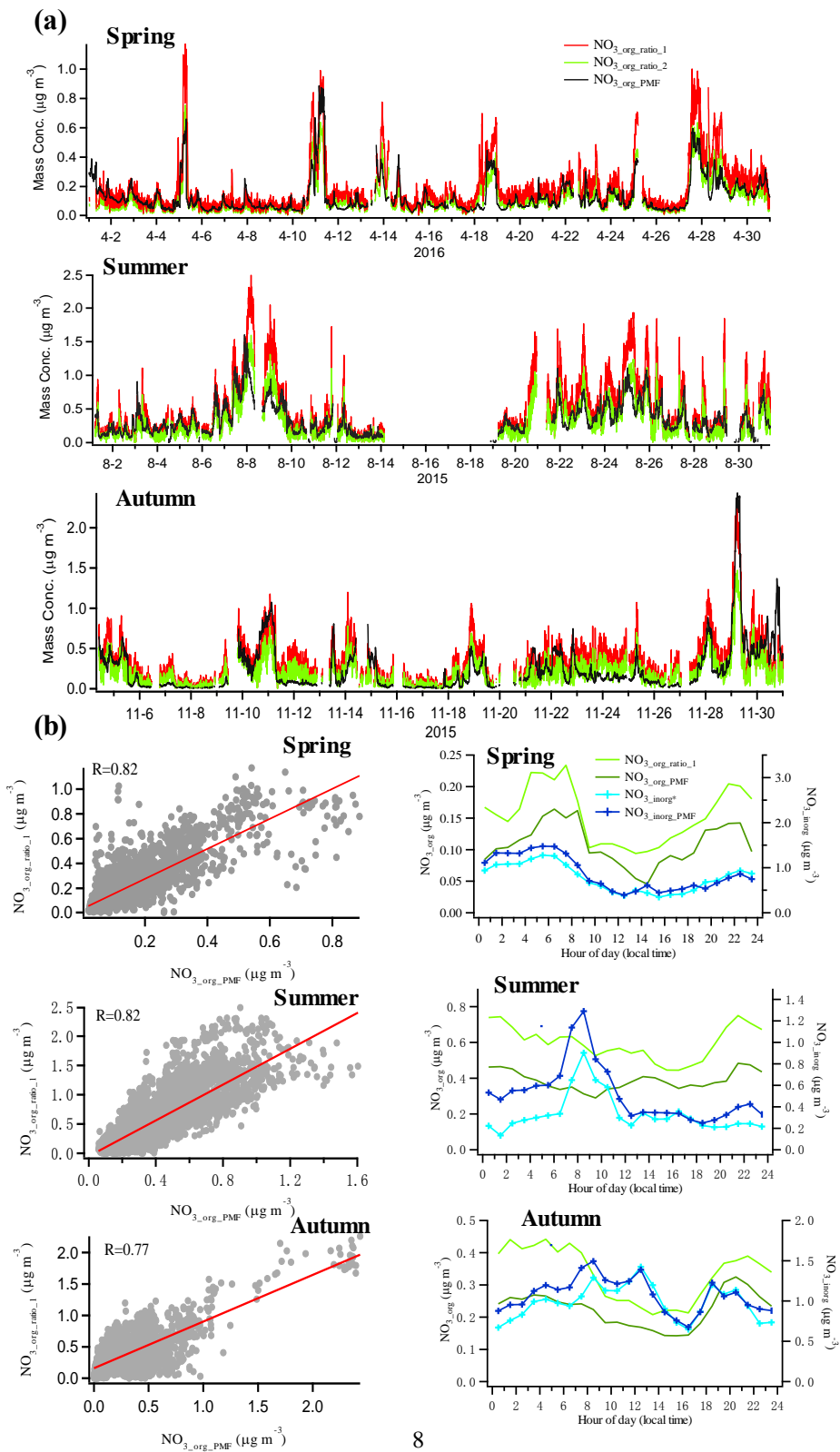
Figure 2. (a) Time series of $NO_{3, org}$ concentration estimated by the NO^+/NO_2^+ ratio method and PMF method for each season; (b) correlations between $NO_{3\_org\_ratio\_1}$ and $NO_{3\_org\_PMF}$ (left panel); diurnal trends of organic nitrates and $NO_{3, org}$ estimated by the different methods (right panel).

3.2 Correlation between organic nitrates and OA factors

As indicated by the results in the PMF method, the majority of organic nitrates were associated with LO-OOA in spring, summer and autumn in the urban atmosphere in Shenzhen, implying a dominant secondary origin of organic nitrates. To further confirm this relationship, we made the correlation analysis between organic nitrates estimated by the NO^+/NO_2^+ ratio method and the three factors resolved by the PMF analysis with only organic mass spectra in the three seasons. Generally, organic nitrates were found better-correlated with LO-OOA (R=0.69-0.77 in Figure 3) than with HOA and MO-OOA (R=0.03-0.69 in Figures S6-S8), which is consistent with the fact that the majority of organic nitrates were associated with LO-OOA in the PMF method. However, the moderate correlation between organic nitrates and HOA implied possibility of direct emissions of organic nitrates. Furthermore, we found a noticeably improved correlation between LO-OOA and organic nitrates at night (19:00-6:00) and a reduced correlation during the daytime (7:00-18:00) in Figure 3, especially in summer, implying that organic nitrates formation might be more closely related to secondary formation at night.


9
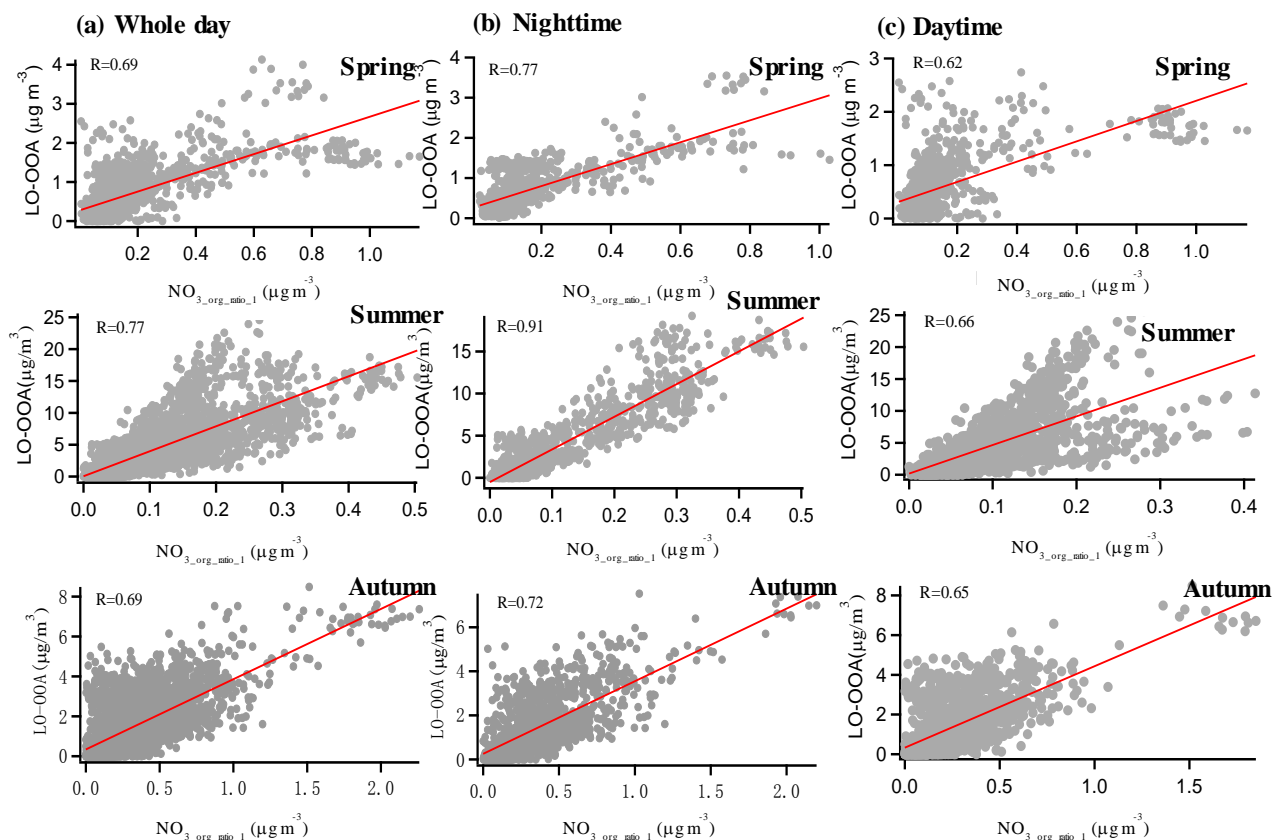
194 **Figure 3.** Correlation of $NO_{3\_org\_ratio\_1}$ and LO-OOA in each season for the whole day (a), at night (b) and in the daytime (c).

195 **3.3 Size distribution characteristics of organic nitrates**

196 In this section, we attempt to use the NO^+/NO_2^+ ratio as an indicator to investigate the size distribution characteristics of organic

197 nitrates. Unfortunately, due to the lack of HR-PToF data, our analyses used the UMR-PToF data of m/z 30 and 46, which

198 might contain the interferences of $CH_2O_X^+$ (Fry et al., 2018). In our case, the time variations of contributions of CH_2O^+ in m/z

199 30 and $CH_2O_2^+$ in m/z 46 in the HR data of PM_1 for the four seasons are shown in Figure S10. For all the four seasons, the

200 average contributions of $CH_2O_X^+$ in m/z 30 and 46 in the HR data of PM_1 were less than 10%, suggesting that the m/z 30/m/z

201 46 ratio could mostly represent the NO^+/NO_2^+ ratio. The average size distributions of m/z 30 and m/z 46 for the four seasons

202 are shown in Figure S11, and Figure 4a shows the average size distributions of different aerosol species and the m/z 30/m/z 46

203 ratio in the four seasons. It is clearly found that the m/z 30/m/z 46 ratio exhibited a decreasing trend in spring, summer and

204 autumn, while it kept constant in winter, similar to the value of R_{NH4NO3} (red dotted line in Figure 4a). In addition, in spring,

205 summer and autumn, the lowest values of the m/z 30/m/z 46 ratio, occurring at ~1 μm, were approximate to the corresponding

206 seasonal values of R_{NH4NO3}. It should be noted that the similar size distribution patterns of the m/z 30/m/z 46 ratio under the

207 highest interferences (>15%) and lowest interferences (<5%) of $CH_2O_X^+$, indicated by the HR data of PM_1, for spring, summer

208 and autumn (Figure S12) imply that the size distribution patterns of the m/z 30/m/z 46 ratio were not affected significantly by

209 the interferences of $CH_2O_X^+$. We also used the size distributions of the m/z 30/m/z 46 ratio to separate the size distributions of

210 inorganic and organic nitrates, as shown in Figure S13, and the results indicate that organic nitrates were relatively more

211 concentrated at small sizes compared to inorganic nitrates. Furthermore, the diurnal trends of the size distribution of the m/z

212 30/m/z 46 ratio in spring, summer and autumn in Figure 4b show apparent higher values at small sizes at night, suggesting an

213 important nighttime local origin of organic nitrates. Combining with the analysis in section 3.2, the local nighttime secondary

214 formation of organic nitrates in warmer seasons in the urban polluted atmosphere in Shenzhen is highlighted. This is consistent

215 with the previous findings in the US and Europe that the nighttime NO_3+VOCs reactions serve as an important source for

216 particulate organic nitrates (Rollins et al., 2012; Xu et al., 2015a, 2015b; Fry et al., 2013; Lee et al., 2016). We will then

217 explore the nighttime NO_3+VOCs reactions in Shenzhen in more detail in the following section.
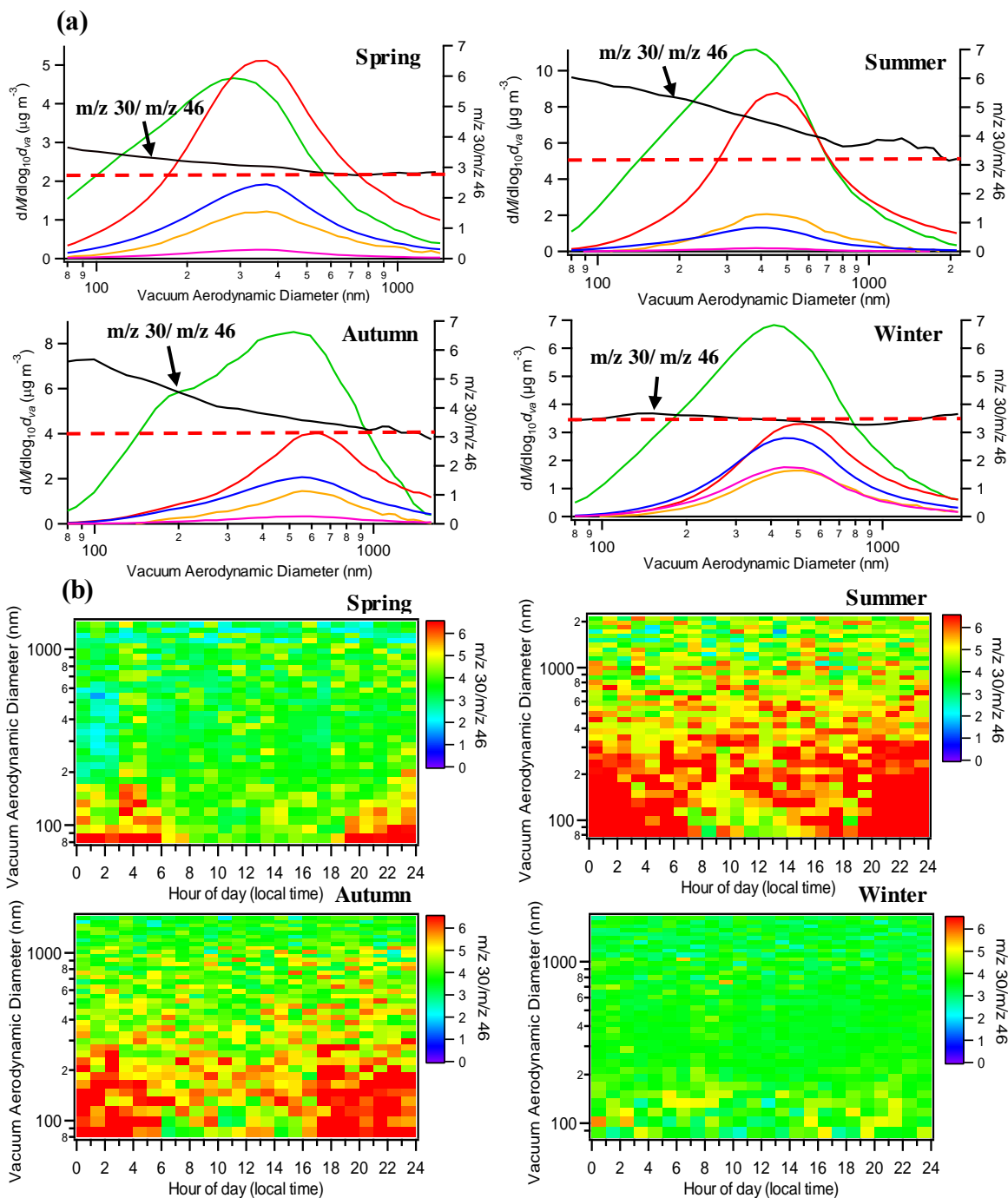
Figure 4. (a) Average size distributions of aerosol species and m/z 30/m/z 46 ratio (red dotted line represents R_{NH4NO3}); (b) diurnal trends of size distribution of m/z 30/m/z 46 ratio.

**3.4 Nighttime particulate organic nitrates formation via NO₃+VOCs**

Since on-line VOCs measurement was only performed during the spring campaign (described in section 2.2), the following theoretical analysis of NO₃+VOCs reactions applies only to the spring case. NO₃+VOCs reactions would yield a large mass of gas- and particle-phase organic nitrates (Rollins et al., 2012; Nah et al., 2016; Boyd et al., 2015, 2017; Xu et al., 2015a, 2015b; Lee et al., 2016). We used Eq. (9) to roughly judge the production potential (PP) of organic nitrates from a NO₃+VOC reaction:

$$[\text{Production Potential}]_{NO3+VOCi} = K_i \cdot [VOC_i] \cdot [NO_3] \quad (9)$$

Where K_i represents the reaction rate coefficient for NO₃ radical and a VOC; $[VOC_i]$ is the concentration of the specific VOC; $[NO_3]$ is the concentration of NO₃ radical. It should be noted that no organic nitrates yield parameter was introduced in Eq. (9), because only a few organic nitrate yields for BVOCs were available in the literature (Fry et al., 2014; Ng et al., 2017). However, given the fact that the values of $K_i \cdot [VOC_i] \cdot [NO_3]$ for different VOC species can differ by orders of magnitude, not multiplying the organic nitrate yields (ranging from 0 to 1) would not significantly affect the PP ranking of VOCs. In the spring campaign, the diurnal variations of NO₂, O₃ and estimated NO₃ radical concentrations are shown in Figure S14. It was found that as a comparison to the nighttime NO₃ radical concentration reported in literature in the United States (Rollins et al., 2012; Xu et al., 2015a), high concentration of NO₂ (19.93±2.31 ppb) at night leaded to high yield of NO₃ radical (1.24±0.76 ppt) in Shenzhen, as calculated in Text S1.

The reaction rate coefficients of typical measured nighttime VOC concentrations with NO₃ radical and the production potentials are listed in Table S3 and shown in Figure 5. These VOCs were considered based on their higher ambient concentrations and availability for reaction kinetics with NO₃ radical. According to the distribution of production potential, five biogenic VOCs (BVOCs) (i.e., α-pinene, limonene, camphene, β-pinene and isoprene) and one anthropogenic VOC (styrene) were identified as notable VOC precursors with high production potential, while the sum of production potential from the other VOCs was negligible as shown in Figure 5b.
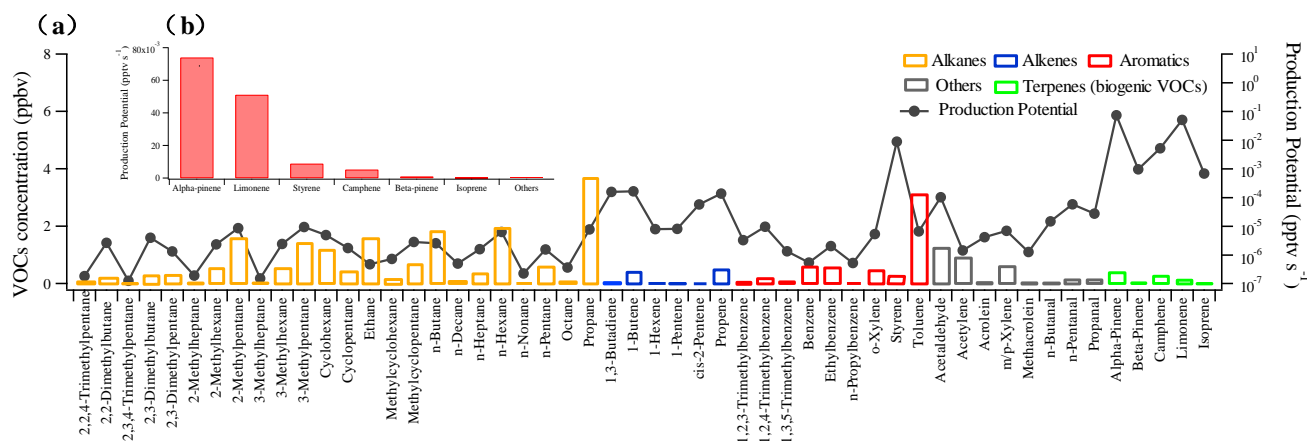
Figure 5. (a) Mean concentrations of VOCs and the corresponding calculated production potential of NO₃+VOC at night during the spring campaign; (b) production potential ranking of VOCs at night during the spring campaign.

245   Based on the production potential evaluation above, we further explore SOA yield of NO_3+the six notable VOC precursors

246   according to the analysis method of particulate organic nitrate formation in Xu et al. (2015a). Briefly, NO_3 and ozone are two

247   main oxidants for SOA formation from VOCs at night. Based on the concentrations of oxidants and the reaction rate constants

248   for VOCs with NO_3 and ozone, the branching ratio of each VOC that reacts with NO_3 can be estimated as in Eq. (10). By

249   combining the estimated branching ratios and SOA yields from chamber studies (Table 3, where the chamber conditions to

250   obtain the yields covered the range of aerosol mass loading in the spring campaign), potential SOA production from these

251   VOCs can be calculated as in Eq. (11) (Xu et al., 2015a):

252
$$branching\ ratio_{species\ i+NO3} = \frac{k_{[species\ i+NO3]} \times [NO_3]}{k_{[species\ i+NO3]} \times [NO_3] + k_{[species\ i+O3]} \times [O_3]}\ (10)$$

253
$$[SOA]_{species,oxidant} = [species] \times branching\ ratio_{species,oxidant} \times yield_{species,oxidant}\ (11)$$

254   The results in Table 3 show that all six notable VOC species were prone to react with NO_3 radical instead of O_3 at night, and

255   the estimated potential SOA production from NO_3+VOCs reactions using SOA mass yields in the literature was 0-0.33 µg m^{-}

256   ^{3} for α-pinene, 0.09-1.28 µg m^{-3} for limonene, 0.24 µg m^{-3} for styrene, 0.004-0.06 µg m^{-3} for β-pinene and 0.002-0.02 µg m^{-3}

257   for isoprene. The SOA yield from camphene is currently unknown in the literature. It is seen that the average observed

258   nighttime concentration of particulate organic nitrates during the spring campaign (0.39-0.83µg m^{-3}, converting $NO_{3.org\_ratio\_1}$,

259    $NO_{3.org\_PMF}$ in Figure 6 into organic nitrates assuming the average molecular weight of organic nitrates of 200 to 300 g mol^{-1})

260   was well within the estimated SOA concentration ranges produced by α-pinene, limonene and styrene in Table 3, indicating

261   that these three VOCs were the key VOC precursors in urban atmosphere in Shenzhen. Considering both the production

262   potentials and SOA yields, the contributions of β-pinene and isoprene to nighttime formation of particulate organic nitrates

263   could be negligible.

264   **Table 3.** Average concentrations, reaction branching and SOA production of α-pinene, limonene, styrene, camphene, β-

265   pinene and isoprene with respect to different oxidants at night in the spring campaign.

Species	Concentration (ppbv)	Rate coefficient [a]		Branching ratio		SOA yield from the literature (with NO_3)	SOA from VOCs + NO_3 (µg m^{-3})
		NO_3	O_3	NO_3	O_3		
α-pinene	0.39	6.64E-12	7.2E-17	0.962	0.038	0-0.16[b]	0-0.33
Limonene	0.14	1.22E-11	1.54E-16	0.957	0.043	0.12-1.74[c]	0.09-1.28
Styrene	0.19	1.50E-12	1.70E-17	0.941	0.059	0.23[d]	0.24
Camphene	0.28	6.20E-13	9.0E-19	0.992	0.008	/	/
β-pinene	0.01	2.51E-12	1.50E-17	0.968	0.032	0.07-1.04[e]	0.004-0.06
Isoprene	0.032	6.96E-13	1.27E-17	0.908	0.091	0.02-0.24 [f]	0.002-0.02

266   [a] Rate coefficients for all species except camphene are from the Master Chemical Mechanism model

267   (http://mcm.leeds.ac.uk/MCM/; under 25 °C), rate coefficients for camphene are from Martínez et al. (1999) and Atkinson et

268   al. (1990).

269   [b] Hallquist et al. (1999); Spittler et al. (2006); Perraud et al. (2010); Fry et al. (2014).

270   [c] Fry et al. (2011, 2014); Spittler et al. (2006); Boyd et al. (2017).

271   [d] Cabrera-Perez et al. (2017).

272   [e] Griffin et al. (1999); Fry et al. (2009); Fry et al. (2014); Boyd et al. (2015).

273   [f] Rollins al. (2009); Ng et al. (2008).

274   The estimation of potential SOA production above suggests significant contributions of α-pinene, limonene, and styrene to

275   SOA, and the significant contribution of camphene is also possible. Thus, we further explore the diurnal variations of the PPs

276   of these four VOCs. Figure 6 shows the diurnal trends of BC, LO-OOA, $NO_{3.org\_ratio\_1}$, $NO_{3.org\_PMF}$, and the PPs of the four

277   VOCs during the spring campaign. There were two apparent nighttime growth periods (i.e., I: 19:00–22:00 and II: 2:00–6:00)

278   for both $NO_{3.org\_ratio\_1}$ and $NO_{3.org\_PMF}$. During Period I, BC maintained a relatively higher level, suggesting stable anthropogenic

279   emissions. In contrast, the increases of all the PPs during Period I indicated that these precursors contributed to the organic

280   nitrate growth. After 22:00, while the PPs still showed a rapid growth, BC and organic nitrates began to decrease, implying

281   possible existence of other important anthropogenic VOC precursors, which were not identified by the GC-FID/MS analysis

282   but would dominate the formation of organic nitrates at this stage. During Period II, the anthropogenic emissions remained at

283   a stable lower level, as indicated by BC, while all the PPs increased with organic nitrates again, indicating that these four

284   precursors also contributed to, or could dominate, this organic nitrate growth. As shown in Figure S15, organic nitrates

285   correlated better with the PPs (R=0.63–0.74) than with LO-OOA (R=0.19–0.31) or BC (R=0.02–0.05) during Period II at the

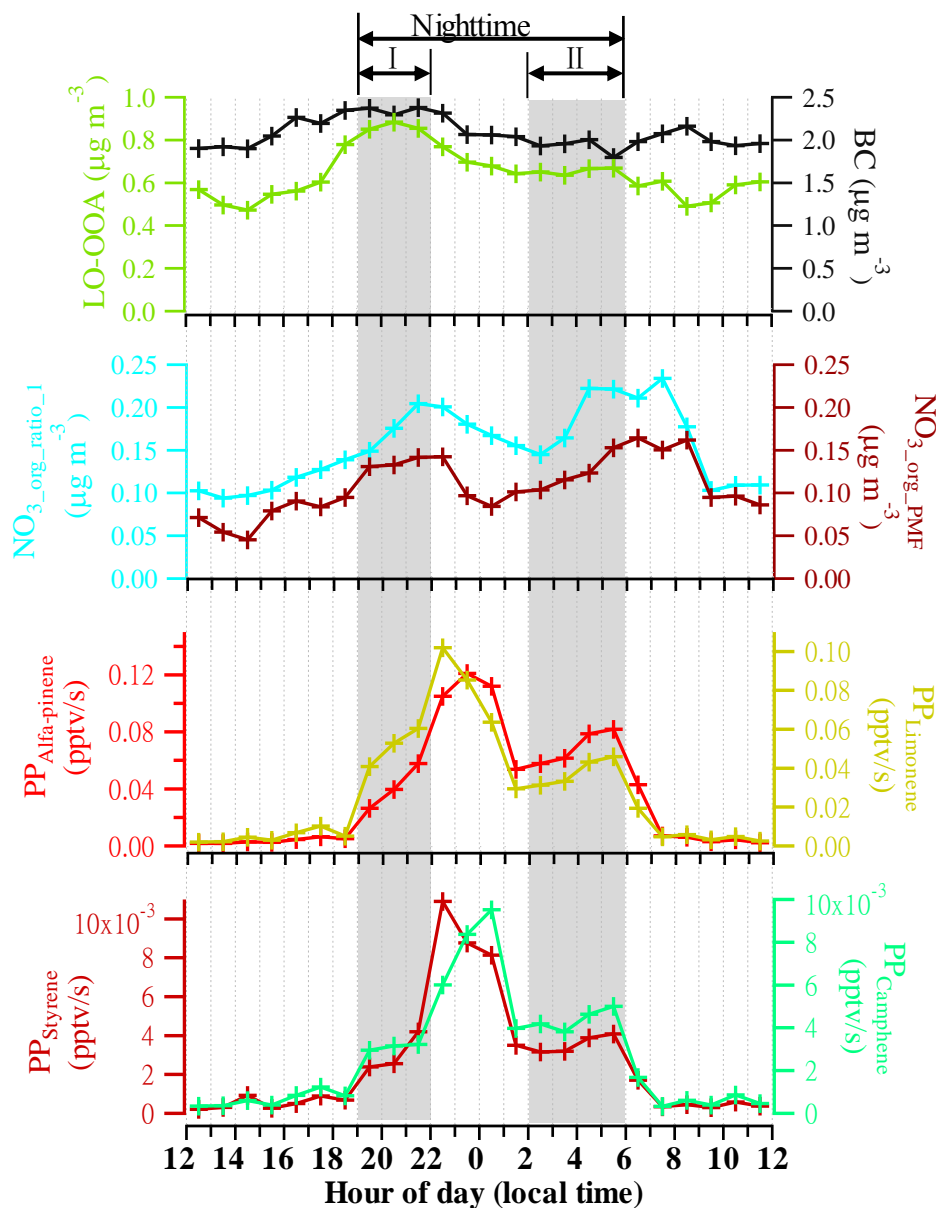286   spring campaign, suggesting the significant contributions of the NO_3 reactions with these precursors.

Figure 6. Diurnal trends of BC, LO-OOA, $NO_{3.org\_ratio\_1}$, $NO_{3.org\_PMF}$ and production potential (PP) of α-pinene, limonene, styrene, and camphene during the spring campaign.

It should be noted that, all previous studies on nighttime organic nitrates formation in the US and Europe focused on mechanisms of NO_3 reactions with BVOCs (Hallquist et al., 1999; Spittler et al., 2006; Perraud et al., 2010; Fry et al., 2014; Nah et al., 2016; Boyd et al., 2015, 2017). In this study, however, we found that anthropogenic VOCs could also play significant roles in particulate organic nitrate formation at night. Besides styrene, one of major aromatics (Cabrera-Perez et al., 2016), there were also other important anthropogenic VOC precursors that we did not identify in the spring campaign. In China,

15

styrene has been actually identified as an important VOC of non-methane hydrocarbons (NMHCs) in urban areas, and has a notable contribution to ozone formation and SOA production (An et al., 2009; Yuan et al., 2013; Zhu et al., 2019). This study highlights the possible key roles of anthropogenic VOC precursors in nighttime particulate organic nitrate formation in urban atmosphere in China, and relevant smog chamber studies for anthropogenic VOCs+NO$_3$ reactions are needed to support parameterization in modeling.

3.5 Comparison with other similar studies and implications

Table 4 shows the average ambient temperatures, average concentrations of NO, NO$_2$, monoterpenes, NO$_{3,org}$, the ratio of NO$_{3,org}$ to NO$_{3,total}$ and the ratio of organic nitrates to total organics in several similar field campaigns available in the literature, which implies the key role of NO$_3$+VOCs reactions for nighttime particulate organic nitrate formation. In general, the variation of the particulate organic nitrates concentration is within an order of magnitude (0.06-0.98 μg/m^3) among the different sites. Higher concentrations of particulate organic nitrates generally are associated with higher NOx concentrations rather than BVOC concentrations. On the other hand, although the BVOCs concentrations in Bakersfield were far less than that in other campaigns, the concentration of particulate organic nitrates there showed an intermediate level among all the campaigns. Therefore, it is suggested that the formation of particulate organic nitrates may be more relevant with NOx than BVOCs, which is consistent with the finding that the organic nitrate production was dominated by NOx in the southeastern US (Edwards et al., 2017). In the spring campaign of this study, we examined the correlation between organic nitrates and NO$_2$ or VOCs (by the sum of α pinene, limonene, camphene and styrene) at night (Figure S16) and found a significant correlation of organic nitrates with NO$_2$ (R=0.40-0.47) rather than with VOCs (R=0.22-0.23), which further suggests that the organic nitrates formation was driven by the NOx-involved NO$_3$ chemistry.

Table 4. Average ambient temperatures, average concentrations of monoterpenes, $NO_{3,total}$, $NO_{3,org}$, $NO_{3,org}$/ $NO_{3,total}$ and the ratio of organic nitrates to total organics (ON/Org) for different field campaigns around the world. The ON results at the European and US sites are from Kiendler-Scharr et al. (2016) and Ng et al. (2017).

Sampling site	Site type	Sampling period	Temperature (°C)	NO (ppbv)	NO₂ (ppbv)	Monoterpenes (ppbv)	NO₃,org (µg m⁻³)	NO₃,org/ NO₃,total	ON/Org	Reference/Note
Bakersfield, **US**	rural	May-June, 2010	23.0		8.2	0.045 (α-pinene) 0.004 (β-pinene) 0.034 (limonene)	0.16	0.28	0.23	Rollins et al. (2012)/ NO3,org measured by TD-LIF
Woodland Park, **US**	high attitude	July-August, 2011	15.0		1.2	0.25 (monoterpene)	0.06	0.86	0.09	Fry et al. (2013)/ Use AMS data to estimate NO3,org
Centreville, **US**	rural	June-July, 2013	24.7	0.1	1.1	0.350 (α-pinene)* 0.312 (β-pinene)* 0.050 (limonene)*	0.08	1.00	0.10	Xu et al. (2015a) Xu et al. (2015b)/ Use AMS data to estimate NO3,org
Barcelona, **Spain**	urban	March, 2009	13.3	11.0	23.6	0.423 (monoterpene)	0.48	0.13	0.13	Mohr et al. (2012) Pandolfi et al. (2014) / Use AMS data to estimate NO3,org
Shenzhen, **China**	urban	April, 2016	24.5	8.0	19.4	0.391 (α-pinene)* 0.013 (β-pinene)* 0.137 (limonene)*	0.16	0.17	0.11	This study/ Use AMS data to estimate NO3,org

*BVOC concentration at night.

17

4. Conclusions

An Aerodyne HR-ToF-AMS was deployed in urban Shenzhen for about one month per season during 2015–2016 to characterize particulate organic nitrates with high time resolution. We discovered high mass fractions of organic nitrates in total organics during warmer seasons, including spring (9-21%), summer (11-25%) and autumn (9-20%), while particulate organic nitrates were negligible in winter. The correlation analysis between organic nitrates and each OA factor showed high correlation (R=0.77 in spring, 0.91 in summer and 0.72 in autumn) between organic nitrates and LO-OOA at night. The diurnal trend analysis of size distribution of m/z 30/m/z 46 ratio further suggested that organic nitrates formation mainly occurred at night. It also suggested that organic nitrates concentrated at smaller sizes, indicating that they were mostly local products. The calculated theoretical nighttime production potential of NO_3 reacting with VOCs measured in spring showed that six VOC species (i.e., α-pinene, limonene, styrene, camphene, β-pinene and isoprene) were prominent precursors. The SOA yield analysis and the nighttime variation of production potential further indicated that α-pinene, limonene, camphene and styrene could contribute significantly to nighttime formation of particulate organic nitrates in spring in Shenzhen, highlighting the unique contribution of anthropogenic VOCs as a comparison to that documented in previous studies in the US and Europe. Finally, the comparison of the results in this study with other similar studies implied that nighttime formation of particulate organic nitrates is more relevant with NOx levels.

Author contributions.

Xiao-Feng Huang designed the research. Kuangyou Yu and Qiao Zhu conducted data analysis and wrote the paper. Ke Du contributed to modelling and writing.

References

An, J. L., Wang, Y. S., Sun, Y.: Effects of nonmethane hydrocarbons on ozone formation in Beijing. Ecology & Environmental Sciences.

Atkinson, R., Aschmann, S. M., Arey, J.: Rate constants for the gas-phase reactions of OH and NO3 radicals and O3 with sabinene and camphene at 296±2 K. Atmospheric Environment. Part A. General Topics, 24, (10), 2647-2654, https://doi.org/10.1016/0960-1686(90)90144-C, 1990

345 Ayres, B.R., Allen, H.M., Draper, D.C., Brown, S.S., Wild, R.J., Jimenez, J.L., Day, D.A., Campuzano-Jost, P., Hu, W., De
346   Gouw, J.A., Koss, A., Cohen, R.C., Duffey, K.C., Romer, P., Baumann, K., Edgerton, E., Takahama, S., Thornton, J.A.,
347   Lee, B.H., Lopez-Hilfiker, F.D., Mohr, C., Wennberg, P.O., Nguyen, T.B., Teng, A.P., Goldstein, A.H., Olson, K., Fry,
348   J.L.: Organic nitrate aerosol formation via NO3+ biogenic volatile organic compounds in the southeastern United States.
349   Atmos. Chem. Phys. 15, 13377-13392. https://doi.org/10.5194/acp-15-13377-2015, 2015.

350 Boyd, C.M., Nah, T., Xu, L., Berkemeier, T., Ng, N.L.: Secondary Organic Aerosol (SOA) from Nitrate Radical Oxidation of
351   Monoterpenes: Effects of Temperature, Dilution, and Humidity on Aerosol Formation, Mixing, and Evaporation. Environ.
352   Sci. Technol. 51, 7831–7841. https://doi.org/10.1021/acs.est.7b01460, 2017.

353 Boyd, C.M., Sanchez, J., Xu, L., Eugene, A.J., Nah, T., Tuet, W.Y., Guzman, M.I., Ng, N.L.: Secondary organic aerosol
354   formation from the β-pinene+NO3 system: effect of humidity and peroxy radical fate. Atmos. Chem. Phys. 15, 7497-
355   7522. https://doi.org/10.5194/acp-15-7497-2015, 2015.

356 Bruns, E.A., Perraud, V., Zelenyuk, A., Ezell, M.J., Johnson, S.N., Yu, Y., Imre, D., Finlayson-Pitts, B.J., Alexander, M.L.:
357   Comparison of FTIR and particle mass spectrometry for the measurement of particulate organic nitrates. Environ. Sci.
358   Technol. 44, 1056-1061. https://doi.org/10.1021/es9029864, 2010.

359 Cabrera-Perez, D., Taraborrelli, D., Sander, R., and Pozzer, A.: Global atmospheric budget of simple monocyclic aromatic
360   compounds, Atmos. Chem. Phys., 16, 6931-6947, https://doi.org/10.5194/acp-16-6931-2016, 2016.

361 Cabrera-Perez, D., Taraborrelli, D., Lelieveld, J., Hoffmann, T., and Pozzer, A.: Global impact of monocyclic aromatics on
362   tropospheric composition, Atmos. Chem. Phys. Discuss., https://doi.org/10.5194/acp-2017-928, 2017.

363 Canagaratna, M.R., Jayne, J.T., Jimenez, J.L., Allan, J.D., Alfarra, M.R., Zhang, Q., Onasch, T.B., Drewnick, F., Coe, H.,
364   Middlebrook, A., Delia, A., Williams, L.R., Trimborn, A.M., Northway, M.J., DeCarlo, P.F., Kolb, C.E., Davidovits, P.,
365   Worsnop, D.R.: Chemical and microphysical characterization of ambient aerosols with the aerodyne aerosol mass
366   spectrometer. Mass Spectrom. Rev. 26, 185-222. https://doi.org/10.1002/mas.20115, 2007.

367 Cubison, M. J., Ortega, A. M., Hayes, P. L., Farmer, D. K., Day, D., Lechner, M. J., Brune, W. H., Apel, E., Diskin, G. S.,
368   Fisher, J. A., Fuelberg, H. E., Hecobian, A., Knapp, D. J., Mikoviny, T., Riemer, D., Sachse, G. W., Sessions, W., Weber,
369   R. J., Weinheimer, A.J., Wisthaler, A., and Jimenez, J. L.: Effects of aging on organic aerosol from open biomass burning
370   smoke in aircraft and laboratory studies, Atmos. Chem. Phys., 11, 12049-12064, https://doi.org/10.5194/acp-11-12049-
371   2011, 2011.

372 Day, D. A., Liu, S., Russell, L. M., and Ziemann, P. J.: Organonitrate group concentrations in submicron particles with high
373   nitrate and organic fractions in coastal southern California, Atmos. Environ., 44, 1970–1979,
374   https://doi.org/10.1016/j.atmosenv.2010.02.045, 2010.

375 DeCarlo, P.F., Kimmel, J.R., Trimborn, A., Northway, M.J., Jayne, J.T., Aiken, A.C., Gonin, M., Fuhrer, K., Horvath, T.,
376   Docherty, K.S., Worsnop, D.R., Jimenez, J.L.: Field-deployable, high-resolution, time-of-flight aerosol mass
377   spectrometer. Anal. Chem. 78, 8281-8289. https://doi.org/10.1021/ac061249n, 2006.

378   Edwards, P. M.; Aikin, K. C.; Dube, W. P.; Fry, J. L.; Gilman, J. B.; de Gouw, J. A.; Graus, M. G.; Hanisco, T. F.; Holloway,
379   J.; Hübler, G.; Kaiser, J.; Keutsch, F. N.; Lerner, B. M.; Neuman, J. A.; Parrish, D. D.; Peischl, J.; Pollack, I. B.;
380   Ravishankara, A. R.; Roberts, J. M.; Ryerson, T. B.; Trainer, M.; Veres, P. R.; Wolfe, G. M.; Warneke, C.; Brown, S. S.:
381   Transition from high- to low-NO_x control of night-time oxidation in the southeastern US. Nature Geoscienc, 10, (7), 490-
382   495. https://doi.org/10.1038/ngeo2976, 2017.

383   Farmer, D.K., Matsunaga, A., Docherty, K.S., Surratt, J.D., Seinfeld, J.H., Ziemann, P.J., Jimenez, J.L.: Response of an aerosol
384   mass spectrometer to organonitrates and organosulfates and implications for atmospheric chemistry. Proc. Natl. Acad.
385   Sci. 107, 6670-6675. https://doi.org/10.1073/pnas.0912340107, 2010.

386   Fry, J. L., Brown, S. S., Middlebrook, A. M., Edwards, P. M., Campuzano-Jost, P., Day, D. A., Jimenez, J. L., Allen, H. M.,
387   Ryerson, T. B., Pollack, I., Graus, M., Warneke, C., de Gouw, J. A., Brock, C. A., Gilman, J., Lerner, B. M., Dubé, W.
388   P., Liao, J., and Welti, A.: Secondary organic aerosol (SOA) yields from NO_3 radical + isoprene based on nighttime
389   aircraft power plant plume transects, Atmos. Chem. Phys., 18, 11663-11682, https://doi.org/10.5194/acp-18-11663-2018,
390   2018.

391   Fry, J.L., Draper, D.C., Barsanti, K.C., Smith, J.N., Ortega, J., Winkler, P.M., Lawler, M.J., Brown, S.S., Edwards, P.M.,
392   Cohen, R.C.: Secondary Organic Aerosol Formation and Organic Nitrate Yield from NO_3 Oxidation of Biogenic
393   Hydrocarbons. Environ. Sci. Technol. 48, 11944–11953. https://doi.org/10.1021/es502204x, 2014.

394   Fry, J.L., Draper, D.C., Zarzana, K.J., Campuzano-Jost, P., Day, D.A., Jimenez, J.L., Brown, S.S., Cohen, R.C., Kaser, L.,
395   Hansel, A., Cappellin, L., Karl, T., Hodzic Roux, A., Turnipseed, A., Cantrell, C., Lefer, B.L., Grossberg, N.:
396   Observations of gas- and aerosol-phase organic nitrates at BEACHON-RoMBAS 2011. Atmos. Chem. Phys. 13, 8585-
397   8605. https://doi.org/10.5194/acp-13-8585-2013, 2013.

398   Fry, J.L., Kiendler-Scharr, A., Rollins, A.W., Brauers, T., Brown, S.S., Dorn, H.P., Dubé, W.P., Fuchs, H., Mensah, A., Rohrer,
399   F., Tillmann, R., Wahner, A., Wooldridge, P.J., Cohen, R. C.: SOA from limonene: Role of NO_3 in its generation and
400   degradation. Atmos. Chem. Phys. 11, 3879-3894. https://doi.org/10.5194/acp-11-3879-2011, 2011.

401   Fry, J.L., Kiendlerscharr, A., Rollins, A.W., Wooldridge, P.J., Brown, S.S., Fuchs, H., Dube, W.P., Mensah, A., Dal Maso,
402   M., Tillmann, R.: Organic nitrate and secondary organic aerosol yield from NO 3 oxidation of β-pinene evaluated using
403   a gas-phase kinetics/aerosol partitioning model. Atmos. Chem. Phys. 9, 1431–1449. https://doi.org/10.5194/acp-9-1431-
404   2009, 2009.

405   Griffin, R. J., Cocker, D. R., III, Flagan, R. C., and Seinfeld, J. H.: Organic aerosol formation from the oxidation of biogenic
406   hydrocarbons. J. Geophys. Res., 104, 3555–3567, https://doi.org/10.1029/1998jd100049, 1999.

407   Hallquist, M., Wängberg, I., Ljungström, E., Barnes, I., Becker, K.H.: Aerosol and product yields from NO_3radical-initiated
408   oxidation of selected monoterpenes. Environ. Sci. Technol. 33, 553-559. https://doi.org/10.1021/es980292s, 1999.

409   Hao, L.Q., Kortelainen, A., Romakkaniemi, S., Portin, H., Jaatinen, A., Leskinen, A., Komppula, M., Miettinen, P., Sueper,
410   D., Pajunoja, A., Smith, J.N., Lehtinen, K.E.J., Worsnop, D.R., Laaksonen, A., Virtanen, A.: Atmospheric submicron

aerosol composition and particulate organic nitrate formation in a boreal forestland-urban mixed region. Atmos. Chem. Phys. 14, 13483-13495. https://doi.org/10.5194/acp-14-13483-2014, 2014.

He, L.Y., Huang, X.F., Xue, L., Hu, M., Lin, Y., Zheng, J., Zhang, R., Zhang, Y.H.: Submicron aerosol analysis and organic source apportionment in an urban atmosphere in Pearl River Delta of China using high-resolution aerosol mass spectrometry. J. Geophys. Res. Atmos. 116, D12. https://doi.org/10.1029/2010JD014566, 2011.

Huang, X.F., He, L.Y., Hu, M., Canagaratna, M.R., Sun, Y., Zhang, Q., Zhu, T., Xue, L., Zeng, L.W., Liu, X.G., Zhang, Y.H., Jayne, J.T., Ng, N.L., Worsnop, D.R.: Highly time-resolved chemical characterization of atmospheric submicron particles during 2008 Beijing Olympic games using an aerodyne high-resolution aerosol mass spectrometer. Atmos. Chem. Phys. 10, 8933-8945. https://doi.org/10.5194/acp-10-8933-2010, 2010.

Huang, X.F., He, L.Y., Xue, L., Sun, T.L., Zeng, L.W., Gong, Z.H., Hu, M., Zhu, T.: Highly time-resolved chemical characterization of atmospheric fine particles during 2010 Shanghai World Expo. Atmos. Chem. Phys. 12, 4897-4907. https://doi.org/10.5194/acp-12-4897-2012, 2012.

Huang, X.F., Xue, L., Tian, X.D., Shao, W.W., Sun, T. Le, Gong, Z.H., Ju, W.W., Jiang, B., Hu, M., He, L.Y.: Highly time-resolved carbonaceous aerosol characterization in Yangtze River Delta of China: Composition, mixing state and secondary formation. Atmos. Environ. 64, 200-207. https://doi.org/10.1016/j.atmosenv.2012.09.059, 2013.

Jimenez, J. L., Jayne, J. T., Shi, Q., Kolb, C. E., Worsnop, D. R., Yourshaw, I., Seinfeld, J. H., Flagan, R. C., Zhang, X. F., Smith, K. A., Morris, J. W., and Davidovits, P.: Ambient aerosol sampling using the aerodyne aerosol mass spectrometer, J. Geophys. Res.-Atmos., 108, 447–457, https://doi.org/10.1029/2001JD001213, 2003.

Kiendler-Scharr, A., Mensah, A. A., Friese, E., Topping, D., Nemitz, E., Prevot, A. S. H., Äijälä, M., Allan, J., Canonaco, F., Canagaratna, M., Carbone, S., Crippa, M., Dall Osto, M., Day, D. A., De Carlo, P., Di Marco, C. F., Elbern, H., Eriksson, A., Freney, E., Hao, L., Herrmann, H., Hildebrandt, L., Hillamo, R., Jimenez, J. L., Laaksonen, A., McFiggans, G., Mohr, C., O'Dowd, C., Otjes, R., Ovadnevaite, J., Pandis, S. N., Poulain, L., Schlag, P., Sellegri, K., Swietlicki, E., Tiitta, P., Vermeulen, A., Wahner, A., Worsnop, D., and Wu, H. C.: Organic nitrates from night-time chemistry are ubiquitous in the European submicron aerosol, Geophys. Res. Lett., 43, 7735–7744, https://doi:10.1002/2016GL069239, 2016.

Lee, B.H., Mohr, C., Lopez-Hilfiker, F.D., Lutz, A., Hallquist, M., Lee, L., Romer, P., Cohen, R.C., Iyer, S., Kurten, T., Hu, W., Day, D.A., Campuzano-Jost, P., Jimenez, J.L., Xu, L., Ng, N.L., Guo, H., Weber, R.J., Wild, R.J., Brown, S.S., Koss, A., de Gouw, J., Olson, K., Goldstein, A.H., Seco, R., Kim, S., McAvey, K., Shepson, P.B., Starn, T., Baumann, K., Edgerton, E.S., Liu, J., Shilling, J.E., Miller, D.O., Brune, W., Schobesberger, S., D'Ambro, E.L., Thornton, J.A.: Highly functionalized organic nitrates in the southeast United States: Contribution to secondary organic aerosol and reactive nitrogen budgets. Proc. Natl. Acad. Sci. 113, 1516-1521. https://doi.org/10.1073/pnas.1508108113, 2016.

Lelieveld, J., Gromov, S., Pozzer, A., Taraborrelli, D.: Global tropospheric hydroxyl distribution, budget and reactivity. Atmos. Chem. Phys. 16, 12477-12493. https://doi.org/10.5194/acp-16-12477-2016, 2016.

443 Martínez, E.; Cabañas, B.; Aranda, A.; Martín, P.; Salgado, S.: Absolute Rate Coefficients for the Gas-Phase Reactions of
444   NO3 Radical with a Series of Monoterpenes at T = 298 to 433 K. Journal of Atmospheric Chemistry, 33, (3), 265-282.
445   https://doi.org/10.1023/A:1006178530211, 1999.

446 Middlebrook, A.M., Bahreini, R., Jimenez, J.L., Canagaratna, M.R.: Evaluation of composition-dependent collection
447   efficiencies for the Aerodyne aerosol mass spectrometer using field data. Aerosol Sci. Technol. 46, 258-271.
448   https://doi.org/10.1080/02786826.2011.620041, 2012.

449 Mohr, C., DeCarlo, P. F., Heringa, M. F., Chirico, R., Slowik, J. G., Richter, R., Reche, C., Alastuey, A., Querol, X., Seco, R.,
450   Peñuelas, J., Jiménez, J. L., Crippa, M., Zimmermann, R., Baltensperger, U., and Prévôt, A. S. H.: Identification and
451   quantification of organic aerosol from cooking and other sources in Barcelona using aerosol mass spectrometer data,
452   Atmos. Chem.Phys., 12, 1649–1665, https://doi.org/10.5194/acp-12-1649-2012, 2012.

453 Nah, T., Sanchez, J., Boyd, C. M., and Ng, N. L.: Photochemical Aging of α-pinene and β-pinene Secondary Organic
454   Aerosol formed from Nitrate Radical Oxidation, Environ. Sci. Technol., 50, 222–231,
455   https://doi:10.1021/acs.est.5b04594 , 2016.

456 Ng, N. L., Brown, S. S., Archibald, A. T., Atlas, E., Cohen, R. C., Crowley, J. N., Day, D. A., Donahue, N. M., Fry, J. L.,
457   Fuchs, H., Griffin, R. J., Guzman, M. I., Herrmann, H., Hodzic, A., Iinuma, Y., Jimenez, J. L., Kiendler-Scharr, A., Lee,
458   B. H., Luecken, D. J., Mao, J., McLaren, R., Mutzel, A., Osthoff, H. D., Ouyang, B., Picquet-Varrault, B., Platt, U., Pye,
459   H. O. T., Rudich, Y., Schwantes, R. H., Shiraiwa, M., Stutz, J., Thornton, J. A., Tilgner, A., Williams, B. J., and Zaveri,
460   R. A.: Nitrate radicals and biogenic volatile organic compounds: oxidation, mechanisms, and organic aerosol, Atmos.
461   Chem. Phys., 17, 2103-2162, https://doi.org/10.5194/acp-17-2103-2017, 2017.

462 Ng, N. L., Canagaratna, M. R., Zhang, Q., Jimenez, J. L., Tian, J., Ulbrich, I. M., Kroll, J. H., Docherty, K.S., Chhabra, P.S.,
463   Bahreini, R., Murphy, S.M., Seinfeld, J.H., Hildebrandt, L., Donahue, N.M., Decarlo, P.F., Lanz, V.A., Prévôt, A.S.H.,
464   Dinar, E., Rudich, Y., Worsnop, D.R.: Organic aerosol components observed in Northern Hemispheric datasets from
465   Aerosol Mass Spectrometry. Atmos. Chem. Phys. 10, 4625-4641. https://doi.org/10.5194/acp-10-4625-2010, 2010.

466 Ng, N. L., Kwan, A. J., Surratt, J. D., Chan, A. W. H., Chhabra, P. S., Sorooshian, A., Pye, H. O. T., Crounse, J. D., Wennberg,
467   P. O., Flagan, R. C., and Seinfeld, J. H.: Secondary organic aerosol (SOA) formation from reaction of isoprene with
468   nitrate radicals (NO3), Atmos. Chem. Phys., 8, 4117–4140, https://doi.org/10.5194/acp-8-4117-2008, 2008.

469 Pandolfi, M.; Querol, X.; Alastuey, A.; Jimenez, J. L.; Jorba, O.; Day, D.; Ortega, A.; Cubison, M. J.; Comerón, A.; Sicard,
470   M.; Mohr, C.; Prévôt, A. S. H.; Minguillón, M. C.; Pey, J.; Baldasano, J. M.; Burkhart, J. F.; Seco, R.; Peñuelas, J.; van
471   Drooge, B. L.; Artiñano, B.; Di Marco, C.; Nemitz, E.; Schallhart, S.; Metzger, A.; Hansel, A.; Lorente, J.; Ng, S.; Jayne,
472   J.; Szidat, S.: Effects of sources and meteorology on particulate matter in the Western Mediterranean Basin: An overview
473   of the DAURE campaign. Journal of Geophysical Research: Atmospheres, 119, (8), 4978-5010.
474   https://10.1002/2013JD021079, 2014.

Perraud, V., Bruns, E. A., Ezell, M. J., Johnson, S. N., Greaves, J., and Finlayson-Pitts, B. J.: Identification of organic nitrates in the NO3 radical initiated oxidation of α-pinene by atmospheric pressure chemical ionization mass spectrometry, Environ. Sci. Technol., 44, 5887–5893. https://doi.org/10.1021/es1005658, 2010.

Rollins, A.W., Browne, E.C., Min, K.-E., Pusede, S.E., Wooldridge, P.J., Gentner, D.R., Goldstein, A.H., Liu, S., Day, D.A., Russell, L.M., Cohen, R.C.: Evidence for NOx Control over Nighttime SOA Formation. Science. 337, 1210-1212. https://doi.org/10.1126/science.1221520, 2012.

Rollins, A. W., Kiendler-Scharr, A., Fry, J. L., Brauers, T., Brown, S. S., Dorn, H.-P., Dubé, W. P., Fuchs, H., Mensah, A., Mentel, T. F., Rohrer, F., Tilmann, R., Wegener, R., Wooldridge, P. J., and Cohen, R. C.: Isoprene oxidation by nitrate radical: alkyl nitrate and secondary organic aerosol yields, Atmos. Chem. Phys., 9, 6685–6703, https://doi.org/10.5194/acp-9-6685-2009, 2009.

Sato, K., Takami, A., Isozaki, T., Hikida, T., Shimono, A., Imamura, T.: Mass spectrometric study of secondary organic aerosol formed from the photo-oxidation of aromatic hydrocarbons. Atmos. Environ. 44, 1080-1087. https://doi.org/10.1016/j.atmosenv.2009.12.013, 2010.

Sobanski, N., Thieser, J., Schuladen, J., Sauvage, C., Song, W., Williams, J., Lelieveld, J., Crowley, J.N.: Day and night-time formation of organic nitrates at a forested mountain site in south-west Germany. Atmos. Chem. Phys. 17, 4115-4130. https://doi.org/10.5194/acp-17-4115-2017, 2017.

Spittler, M., Barnes, I., Bejan, I., Brockmann, K.J., Benter, T., Wirtz, K.: Reactions of NO3 radicals with limonene and α-pinene : Product and SOA formation. Atmos. Environ. 40, 116–127. https://doi.org/10.1016/j.atmosenv.2005.09.093, 2006.

Sun, Y., Zhang, Q., Schwab, J.J., Yang, T., Ng, N.L., Demerjian, K.L.: Factor analysis of combined organic and inorganic aerosol mass spectra from high resolution aerosol mass spectrometer measurements. Atmos. Chem. Phys. 12, 8537–8551. https://doi.org/10.5194/acp-12-8537-2012, 2012.

Teng, A.P., Crounse, J.D., Lee, L., St. Clair, J.M., Cohen, R.C., Wennberg, P.O.: Hydroxy nitrate production in the OH-initiated oxidation of alkenes. Atmos. Chem. Phys. 139, 5367-5377. https://doi.org/10.5194/acp-15-4297-2015, 2015.

Teng, A.P., Crounse, J.D., Wennberg, P.O.: Isoprene Peroxy Radical Dynamics. J. Am. Chem. Soc. 15, 4297-4316. https://doi.org/10.1021/jacs.6b12838, 2017.

Wang, H.; Lu, K.; Chen, X.; Zhu, Q.; Chen, Q.; Guo, S.; Jiang, M.; Li, X.; Shang, D.; Tan, Z.; Wu, Y.; Wu, Z.; Zou, Q.; Zheng, Y.; Zeng, L.; Zhu, T.; Hu, M.; Zhang, Y.: High N_2O_5 Concentrations Observed in Urban Beijing: Implications of a Large Nitrate Formation Pathway. Environmental Science & Technology Letters, 4, (10), 416-420. https://doi.10.1021/acs.estlett.7b00341, 2018.

Wang, M.; Zeng, L.; Lu, S.; Shao, M.; Liu, X.; Yu, X.; Chen, W.; Yuan, B.; Zhang, Q.; Hu, M.; Zhang, Z.: Development and validation of a cryogen-free automatic gas chromatograph system (GC-MS/FID) for online measurements of volatile organic compounds, 6, (23), 9424-9434. Analytical Methods, https://doi.10.1039/C4AY01855A, 2014.

Xu, L., Guo, H., Boyd, C.M., Klein, M., Bougiatioti, A., Cerully, K.M., Hite, J.R., Isaacman-VanWertz, G., Kreisberg, N.M., Knote, C., Olson, K., Koss, A., Goldstein, A.H., Hering, S. V., de Gouw, J., Baumann, K., Lee, S.-H., Nenes, A., Weber, R.J., Ng, N.L.: Effects of anthropogenic emissions on aerosol formation from isoprene and monoterpenes in the southeastern United States. Proc. Natl. Acad. Sci. 112, 37-42. https://doi.org/10.1073/pnas.1417609112, 2015a.

Xu, L., Suresh, S., Guo, H., Weber, R.J., Ng, N.L.: Aerosol characterization over the southeastern United States using high-resolution aerosol mass spectrometry: Spatial and seasonal variation of aerosol composition and sources with a focus on organic nitrates. Atmos. Chem. Phys. 15, 7307-7336. https://doi.org/10.5194/acp-15-7307-2015, 2015b.

Xu, W., Sun, Y., Wang, Q., Du, W., Zhao, J., Ge, X., Han, T., Zhang, Y., Zhou, W., Li, J., Fu, P., Wang, Z., Worsnop, D.R.: Seasonal Characterization of Organic Nitrogen in Atmospheric Aerosols Using High Resolution Aerosol Mass Spectrometry in Beijing, China. ACS Earth Sp. Chem. 1, 673–682. https://doi.org/10.1021/acsearthspacechem.7b00106, 2017.

Yan, C., Nie, W., Äijälä, M., Rissanen, M.P., Canagaratna, M.R., Massoli, P., Junninen, H., Jokinen, T., Sarnela, N., Häme, S.A.K., Schobesberger, S., Canonaco, F., Yao, L., Prévôt, A.S.H., Petäjä, T., Kulmala, M., Sipilä, M., Worsnop, D.R., Ehn, M.: Source characterization of highly oxidized multifunctional compounds in a boreal forest environment using positive matrix factorization. Atmos. Chem. Phys. 16, 12715-12731. https://doi.org/10.5194/acp-16-12715-2016, 2016.

Yuan, B., Hu, W. W., Shao, M., Wang, M., Chen, W. T., Lu, S. H., Zeng, L. M., and Hu, M.: VOC emissions, evolutions and contributions to SOA formation at a receptor site in eastern China, Atmos. Chem. Phys., 13, 8815-8832, https://doi.org/10.5194/acp-13-8815-2013, 2013.

Zhang, Q., Jimenez, J.L., Canagaratna, M.R., Ulbrich, I.M., Ng, N.L., Worsnop, D.R., Sun, Y.: Understanding atmospheric organic aerosols via factor analysis of aerosol mass spectrometry: A review. Anal. Bioanal. Chem. 401, 3045-3067. https://doi.org/10.1007/s00216-011-5355-y, 2011.

Zhang, Y.H., Su, H., Zhong, L.J., Cheng, Y.F., Zeng, L.M., Wang, X.S., Xiang, Y.R., Wang, J.L., Gao, D.F., Shao, M., Fan, S.J., Liu, S.C.: Regional ozone pollution and observation-based approach for analyzing ozone-precursor relationship during the PRIDE-PRD2004 campaign. Atmos. Environ. 42, 6203-6218. https://doi.org/10.1016/j.atmosenv.2008.05.002, 2008.

Zhu, B., Han, Y., Wang, C., Huang, X. F., Xia, S. Y., Niu, Y. B., Yin, Z. X, He, L.Y. : Understanding primary and secondary sources of ambient oxygenated volatile organic compounds in Shenzhen utilizing photochemical age-based parameterization method. Journal of Environmental Sciences, 75, 105-114. https://doi.org/10.1016/j.jes.2018.03.008, 2019.

Zhu, Q., He, L.Y., Huang, X.F., Cao, L.M., Gong, Z.H., Wang, C., Zhuang, X., Hu, M.: Atmospheric aerosol compositions and sources at two national background sites in northern and southern China. Atmos. Chem. Phys. 16, 10283-10297. https://doi.org/10.5194/acp-16-10283-2016, 2016.

540 Zhu, Q., Huang, X.-F., Cao, L.-M., Wei, L.-T., Zhang, B., He, L.-Y., Elser, M., Canonaco, F., Slowik, J. G., Bozzetti, C., El-
541   Haddad, I., and Prévôt, A. S. H.: Improved source apportionment of organic aerosols in complex urban air pollution using
542   the multilinear engine (ME-2), Atmos. Meas. Tech., 11, 1049-1060. https://doi.org/10.5194/amt-11-1049-2018, 2018.